


Broadband Chip-Based Source of Quantum Noise with Electrically Controllable Beam Splitter

E.A. Vashukevich^{1,*}, V.V. Lebedev^{2,3}, I.V. Ilichev^{2,3}, P.M. Agruzov^{2,3}, A.V. Shamrai^{2,3},
V.M. Petrov³ and T.Yu. Golubeva¹

¹*Saint Petersburg State University, Universitetskaya nab. 7/9, St. Petersburg 199034, Russian Federation*

²*Ioffe Institute, Politekhnikeskaya str. 29, St. Petersburg 194021, Russian Federation*

³*ITMO University, Kronverksky pr. 49, St. Petersburg 197101, Russian Federation*

 (Received 20 September 2021; revised 17 April 2022; accepted 6 May 2022; published 22 June 2022)

The theory and practical realization of a broadband quantum-noise generator based on an original integrated optical beam splitter in the form of a Mach-Zehnder interferometer is demonstrated. The beam splitter with a double output, made on a lithium niobate substrate, provides accurate electro-optical balancing of the homodyne quantum-noise detection circuit. The experimentally obtained excess of quantum noise over classical noise is 12 dB in the frequency band over 4 GHz, which is the best parameters of quantum-noise generators known from the literature.

DOI: [10.1103/PhysRevApplied.17.064039](https://doi.org/10.1103/PhysRevApplied.17.064039)

I. INTRODUCTION

Quantum-noise generators and random-number generators based on them are in demand for many applications [1–3]. The homodyne detection of vacuum fluctuations is one of the most efficient techniques to build a quantum-noise generator. As a rule, quantum-noise generators are used for the subsequent development of quantum-random-number generators. To do this, the analog signal must be converted into a digital code [4–14].

It is also worthwhile to note that quantum-noise generators belong to a wide class of microwave or rf photonics devices, which have been developing rapidly over the past decade [15]. Therefore, such devices are of interest in areas other than for the generation of digital sequences only.

Quantum vacuum fluctuations are used as a physical source of entropy of the noise generator. Its technical implementation is based on a local oscillator, beam splitter, and balanced detection scheme, that provides suppression of classical noise and registration of quantum shot noise. From the point of view of the informational throughput of the random-number generator, one of the most useful parameters here is the frequency band of the quantum noise at the output of the balanced detector [6]. The currently experimentally achieved maximum band of homodyne detection of vacuum fluctuations is about 1 GHz [8,9], which is due to the use of schemes on the so-called “volumetric” optics.

The integrated optical design provides much better mechanical and temperature stability compared to the volumetric or fiber-optic implementation. The use of electro-optical lithium niobate (LiNbO₃) allows fast and accurate adjustment of the interferometer arm, as well as use of high light powers (hundreds of milliwatts), which is very helpful for obtaining a high level of quantum noise, which is proportional to the intensity of light.

Integrated optical beam splitters based on silicon optical waveguides [10] can only partially solve the problems of volumetric optics. Sufficiently high absorption and photosensitivity at telecommunications wavelengths (1500–1600 nm) produce sources of additional classical noise and limit the maximum optical power, and the thermoelectric control used in Ref. [10] for active tuning has a high inertia and is not suitable for broadband devices. This did not allow the generation of quantum noise in the band of more than 150 MHz.

To construct a quantum-noise generator, a scheme based on balanced homodyne detection of a vacuum field is widely used. However, such an implementation of the generator has a significant limitation: the lack of the ability to control interference when mixing fields on the beam splitter. Violation of the ideal symmetry of the beam-splitter coefficients leads to a violation of the balance on the detectors, which negatively affects the visibility of the signal, and, as a result, the speed of random-number generation. To solve this problem and implement the control of the balanced detector, we use an integrated optical Mach-Zehnder interferometer formed by input *Y* branch, output *X* coupler, and with the electro-optical control of phase difference between arms of the interferometer.

*e.vashukevich@spbu.ru

Note that the Y branch despite the presence of only one input port (Fig. 1) serves as a mixer of fields of a local oscillator and vacuum fluctuations. Vacuum fluctuations penetrate in the Y branch from the substrate as leakage modes. It is not difficult to prove that there is a second port, given the unitarity of conversion of the input radiation to the output produced by the beam splitter. By organizing the illumination of the circuit from the output side and varying the phase difference of the fields, it is possible to see the points of the output radiation through the substrate in a situation where the central mode is suppressed by destructive interference. It is these output points that will correspond to the second, unlit (vacuum) input of the beam splitter when the circuit is normally illuminated from left to right. Thus, we describe the input Y branch of the scheme under consideration as a four-port device [16] like a X coupler or volume beam splitter, on one of the ports of which there is a field in the vacuum state. Then the whole system under consideration is similar to the “usual” Mach-Zehnder interferometer with two inputs and two outputs.

II. THEORY

Although the actual experimental scheme corresponds to that shown in Fig. 1(c), we can formally describe Y branch as an X coupler, as noted in the Introduction, meaning the input vacuum modes penetrate the interferometer’s input through the substrate. Let us consider the case when the strong classic field from the local oscillator $E_{LO}(z, t)$ enters the beam splitter at input 1, and only the vacuum field $\hat{E}_{vac}(z, t)$ enters at input 2 [Fig. 1(c)]. After mixing on the first beam splitter, the fields are given a relative phase delay ϕ , after which the fields are mixed again on the second beam splitter and detected. It is the phase difference ϕ that acts as a parameter that additionally controls the interference conditions on the second beam splitter. The transformation of the fields on the first and second beam

splitters can be set by matrices $M_{BS,1}, M_{BS,2}$:

$$M_{BS,i} = \begin{pmatrix} \cos(\alpha_i) & \sin(\alpha_i) \\ \sin(\alpha_i) & -\cos(\alpha_i) \end{pmatrix}, \quad i = 1, 2. \quad (1)$$

Here the parameters α_1, α_2 are set so the $\cos(\alpha_i)$ is equal to the amplitude transmission coefficient of the beam splitter t_i , and the $\sin(\alpha_i)$ is correspondingly equal to the reflection coefficient r_i . It can be noted that with the chosen parametrization, the conservation law $r_i^2 + t_i^2 = 1$ is fulfilled automatically.

The phase delay in one of the arms of the interferometer is given by the matrix:

$$M_{Ph} = \begin{pmatrix} \exp\{i\phi/2\} & 0 \\ 0 & \exp\{-i\phi/2\} \end{pmatrix}. \quad (2)$$

Next, one can write down the expression for the fields at the output of the scheme $\hat{E}_{out,1}, \hat{E}_{out,2}$ in terms of the initial fields:

$$\begin{pmatrix} \hat{E}_{out,1} \\ \hat{E}_{out,2} \end{pmatrix} = U \begin{pmatrix} E_{LO} \\ \hat{E}_{vac} \end{pmatrix} \quad (3)$$

$$U = M_{BS,2} \times M_{Ph} \times M_{BS,1}. \quad (4)$$

Here and below, hats denote quantum-mechanical operators. The elements of the transformation matrix are

$$U_{11} = e^{i\phi/2} (\cos(\alpha_1) \cos(\alpha_2) + e^{-i\phi} \sin(\alpha_1) \sin(\alpha_2)), \quad (5)$$

$$U_{12} = e^{i\phi/2} (\sin(\alpha_1) \cos(\alpha_2) - e^{-i\phi} \cos(\alpha_1) \sin(\alpha_2)), \quad (6)$$

$$U_{21} = e^{i\phi/2} (\cos(\alpha_1) \sin(\alpha_2) - e^{-i\phi} \sin(\alpha_1) \cos(\alpha_2)), \quad (7)$$

$$U_{22} = e^{-i\phi/2} (\cos(\alpha_1) \cos(\alpha_2) + e^{i\phi} \sin(\alpha_1) \sin(\alpha_2)). \quad (8)$$

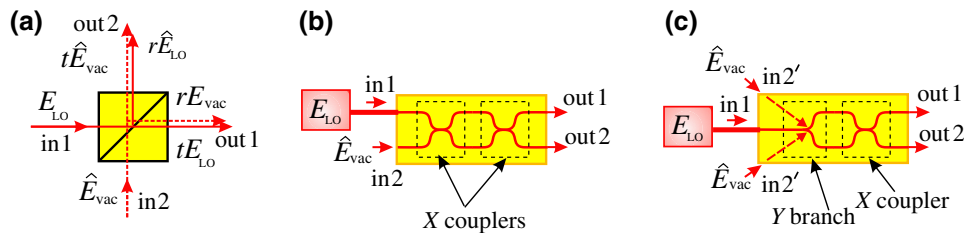


FIG. 1. (a) Definition of the coefficients r_i and t_i for the volumetric beam splitter cube. (b),(c) The possible types of tunable integrated optical beam splitters. (b) Beam splitter, based on two X couplers, that form the Mach-Zehnder interferometer with two inputs and two outputs; input 1 is directly connected by optical fiber to the source of E_{LO} , only the mode of the local oscillator gets to this input; input 2 is open, only the modes of vacuum fluctuations corresponding to the modes of the optical waveguide enters this input; (c) based on one Y branch and one X coupler, that form the Mach-Zehnder interferometer with one input and two outputs. The additional, second input $in2'$ for vacuum fluctuations occurs due to the leakage modes (dashed arrows).

The photocurrent operators on both detectors can be written as follows:

$$\hat{j}_1 = \hat{E}_{\text{out},1}^\dagger \hat{E}_{\text{out},1} = (U_{11}^* E_{\text{LO}}^* + U_{12}^* \hat{E}_{\text{vac}}^\dagger) \times (U_{11} E_{\text{LO}} + U_{12} \hat{E}_{\text{vac}}), \quad (9)$$

$$\hat{j}_2 = \hat{E}_{\text{out},2}^\dagger \hat{E}_{\text{out},2} = (U_{21}^* E_{\text{LO}}^* + U_{22}^* \hat{E}_{\text{vac}}^\dagger) \times (U_{21} E_{\text{LO}} + U_{22} \hat{E}_{\text{vac}}). \quad (10)$$

Now, for convenience, let us move on to the quadrature components (with numeric representation for the classical field and operator for the quantum one): $E_{\text{LO}} = \varepsilon' + i\varepsilon''$, $\hat{E}_{\text{vac}} = \hat{x} + i\hat{y}$; in addition, let us denote $|E_{\text{LO}}|^2 = I_{\text{LO}}$. The differential signal $\hat{j}_-(\phi)$ can be written as follows [we denote $\alpha_\pm = 2(\alpha_1 \pm \alpha_2)$]:

$$\begin{aligned} \hat{j}_-(\phi) &= \hat{j}_1 - \hat{j}_2 = [I_{\text{LO}} - \hat{x}^2 - \hat{y}^2] \\ &\times [\cos^2(\phi/2) \cos(\alpha_-) + \sin^2(\phi/2) \cos(\alpha_+)] \\ &+ 2[\varepsilon' \hat{x} + \varepsilon'' \hat{y}] \\ &\times [\cos^2(\phi/2) \sin(\alpha_-) + \sin^2(\phi/2) \sin(\alpha_+)] \\ &- 2[\varepsilon' \hat{y} - \varepsilon'' \hat{x}] \sin(\phi) \sin(2\alpha_2). \end{aligned} \quad (11)$$

In the case when the beam splitters are symmetric $r_i = 1/\sqrt{2} = t_i$, the transformation matrix has a simple form:

$$U = \begin{pmatrix} \cos \phi/2 & i \sin \phi/2 \\ i \sin \phi/2 & \cos \phi/2 \end{pmatrix}. \quad (12)$$

The difference photocurrent with symmetric beam splitters $\hat{j}_^s(\phi)$ will be modulated by the phase difference ϕ :

$$\hat{j}_^s(\phi) = (I_{\text{LO}} - \hat{x}^2 - \hat{y}^2) \cos \phi - 2(\varepsilon' \hat{y} - \varepsilon'' \hat{x}) \sin \phi. \quad (13)$$

As you can see, with the phase difference $\phi = \pi/2$ the first term proportional to the intensity of the fields will be completely suppressed, and homodyne detection of the quadrature components of the quantum field is carried out in the Mach-Zehnder interferometer scheme. For simplicity, here and further, we select the phase of the local oscillator so that $\varepsilon'' = 0$, then the difference signal can be written as follows:

$$\hat{j}_^s(\pi/2) = -2\varepsilon' \hat{y}. \quad (14)$$

Expression (14) shows that with an appropriate choice of the phase difference between the arms of the interferometer, the differential signal will be proportional to the quadrature component of the quantum vacuum field \hat{y} . It is well known that vacuum quadratures have a zero mean value but a nonzero second moment, which means the presence of a quantum-random result of a single measurement.

Thus, we get the possibility to generate a sequence of truly random numbers in the proposed scheme. As can be seen from Eq. (14), the dispersion of the noise field y increases in proportion to the magnitude of the field of the local oscillator.

Now we take into account the differences between the real experimental situation and the ideal one described above. First of all, we take into account the possible asymmetry of the beam splitter. Let us assume that one of the beam splitters (for example, the output one) is asymmetric, choosing $r_2 = 1/\sqrt{2} + d$, $t_2 = \sqrt{1 - (1/\sqrt{2} + d)^2}$, here d is the asymmetry parameter. We can write down the dependence of the difference current in the case of an asymmetric beam splitter $\hat{j}_^a(\phi)$ on the phase, leaving the field of the local oscillator purely real and keeping only linear terms in the small parameter d expansion:

$$\begin{aligned} \hat{j}_^a(\phi) &= \left(1 + \frac{3d}{2\sqrt{2}}\right) \cos(\phi) (I_{\text{LO}}^2 - \hat{x}^2 - \hat{y}^2) \\ &- 2 \left(1 + \frac{3d}{2\sqrt{2}}\right) \sin(\phi) \varepsilon' \hat{y} - 4\sqrt{2}d\varepsilon' \hat{x}. \end{aligned} \quad (15)$$

As one can see, the second quadrature component begins to appear in the signal. Moreover, the last term in Eq. (15) is phase independent. However, the contribution from the first term, proportional to the intensity of the fields, which is most harmful for noise generation, can be completely compensated by choosing a suitable phase of the modulator. When the phase difference is $\phi = \pi/2$ we get

$$\hat{j}_^a\left(\frac{\pi}{2}\right) = -2 \left(1 + \frac{3d}{2\sqrt{2}}\right) \sin(\phi) \varepsilon' \hat{y} - 4\sqrt{2}d\varepsilon' \hat{x}. \quad (16)$$

Note that the obtained form of recording the signal allows us to talk about the measurement of the generalized quadrature of the noise field, that is, the measurement in the basis rotated by some angle. Since the distribution of the vacuum field on the phase plane is absolutely symmetric, the reversal of the basis does not introduce any changes in the operation of the noise generator. Thus, in the absence of other factors of the ‘‘imperfection’’ of the scheme, the asymmetry of the beam splitter would be insignificant for the generation of random numbers.

The key factor here, however, is the fact that if the beam splitter is not symmetric, an additional classical noise component will be present in the difference current, which is completely subtracted when considering a symmetric circuit. We show this explicitly by introducing coefficients η_1, η_2 associated with the presence of classical noise, and $1 - \eta_1, 1 - \eta_2$ is the losses in corresponding arms of the interferometer. Then, instead of Eq. (4) used above, the field at the output of the interferometer will be set by the

expression:

$$\begin{pmatrix} \hat{E}_{\text{out},1} \\ \hat{E}_{\text{out},2} \end{pmatrix} = \tilde{U} \begin{pmatrix} E_{\text{LO}} \\ \hat{E}_{\text{vac}} \end{pmatrix} \quad (17)$$

$$\tilde{U} = M_{\text{BS}\otimes\otimes} \begin{pmatrix} \eta_1 & 0 \\ 0 & \eta_2 \end{pmatrix} M_{\text{Ph}} \times M_{\text{BS},1}. \quad (18)$$

We repeat all the calculations made without taking into account losses, preserving the assumptions made earlier about the symmetry of the first beam splitter and the realness of the field of the local oscillator. The difference current $\hat{j}_-(\phi)$ will then have the form:

$$\begin{aligned} \hat{j}_-(\phi) = & \frac{1}{2} \cos(2\alpha_2) (\eta_1^2 - \eta_2^2) (I_{\text{LO}} + \hat{x}^2 + \hat{y}^2) \\ & + \eta_1 \eta_2 \sin(2\alpha_2) \cos(\phi) (I_{\text{LO}} - \hat{x}^2 - \hat{y}^2) \\ & + \varepsilon' \hat{x} \cos(2\alpha_2) (\eta_1^2 + \eta_2^2) \\ & - 2\eta_1 \eta_2 \varepsilon' \hat{y} \sin(2\alpha_2) \sin(\phi). \end{aligned} \quad (19)$$

In the case of symmetrical output beam splitter $\alpha_2 = \pi/4$, the expression (19) is reduced by the choice of phase $\phi = \pi/2$ to Eq. (14) with extra multiplication by factor $\eta_1 \eta_2$. However, as one can see, for any asymmetric beam splitter in Eq. (19), there remains a phase-independent first term containing the intensity of the field of the local oscillator, which will dominate the signal of interest. This term can be removed by analyzing the phase ϕ and selecting it so that the following equation is performed:

$$\cos(\phi) \approx -\frac{(\eta_1^2 - \eta_2^2)}{2\eta_1 \eta_2} \cot(2\alpha_2). \quad (20)$$

Such a choice of the modulator phase leads to complete mutual compensation of the first two terms in expression (19). As a result, the expression for the difference photocurrent can again be represented as the amplification of the generalized noise quadrature [similar to Eq. (15)], where the gain is lesser than the original one by a factor of $\eta_1 \eta_2$. It is interesting to estimate the amount of phase adjustment required for balancing the circuit. The theoretical evaluation shows that, for example, for $\cos(2\alpha_2) = -0.02$, $\eta_1 = 0.9$, $\eta_2 = 0.85$ to compensate for the term containing I_{LO} , we need to add to the phase $\phi = \pi/2$ only the $3 \times 10^{-4}\pi$. However, to obtain the suppression of the I_{LO} terms equal to 10 dB we need the phase precision to be only about 0.02π . The control system we use in this work ensures the accuracy of phase control approximately 0.01π , so the theoretical calculations completely explain the experimental results, shown at the Fig. 4. Thus, the use of a phase modulator makes it possible to balance the circuit in the presence of not only asymmetric detector operation, but also various classical noises in the interferometer channels.

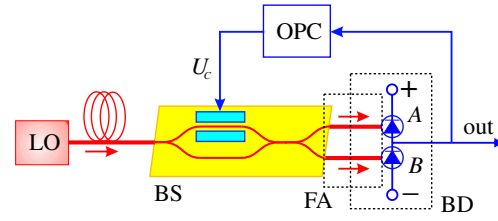


FIG. 2. Experimental realization: quantum-noise generator based on integrated-optic Mach-Zehnder beam splitter with the electrical control. LO is the local oscillator, BS is the beam splitter, FA is the fiber-optic assembly, BD is the balanced detector, OPC is the operating point control system.

III. EXPERIMENT

We propose and experimentally implement a broadband quantum-noise generator using an integrated optical Mach-Zehnder interferometer with a single input and a double output as an electrically controlled beam splitter (BS), made on the basis of optical waveguides in a lithium niobate crystal substrate (Fig. 2). The LiNbO_3 congruent single-crystal plate of the X cut had the size $5 \times 50 \times 1 \text{ mm}^3$. The single-mode channel optical waveguides are manufactured using the technology of thermal diffusion of Ti ions [17]. Light propagated along Y crystallographic axes. A push-pull electrodes is deposited along one of the arms of the interferometer, which made it possible to adjust the amplitude transmission coefficient of the beam splitter t_i using the electro-optical effect.

A single frequency laser with distributed feedback with a wavelength of 1552 nm, a radiation line width of 170 kHz, and a power of 100 mW is used as a local oscillator (LO).

Special attention is paid to the design of the balanced detector (BD). The radiation from the beam-splitter outputs is transmitted through the fiber assembly (FA) to the (In,Ga)As-pin photodiodes (A, B) that form the balanced detector. The difference of the optical paths of the fiber-optic assembly did not exceed 0.1 of the operating wavelength.

The band of each photodiode is 10 GHz, which provides the band of the balanced detector above 4 GHz. For this purpose, photodiodes with the closest possible frequency response and the same sensitivity of approximately equal to 0.78 A/W are selected. A high saturation current (approximately 30 mA) and a dark current of less than $1 \mu\text{A}$ provides a high dynamic range. The operating point control system (OPC) provides accurate balancing of output currents ($< 0.1\%$) [18]. To suppress classical noise, antiphase subtraction of synchronous signals is provided by equalizing the optical and electrical paths in the balanced circuit. It should be noted that for such balancing precision we perform phase adjustment according to expressions (19) and (20) with the precision of 0.001%.

The efficiency of the balanced photodetector is evaluated by suppressing common-mode interference. To emulate the common-mode signal the laser radiation is modulated in amplitude and differential signal is applied to the tunable integrated optical BS. The suppression is defined as the ratio of the frequency response to a differential signal to the frequency response to a common-mode signal. The common-mode interference suppression by more than 15 dB is observed in the band over 3 GHz. The decrease in the suppression efficiency with increasing frequency is due to increased requirements for the accuracy of performing phase matching and the difference in the frequency response of photodiodes.

A part of the electrical signal from the output of the balanced detector is sent to the OPC unit, which generates a feedback signal with a control voltage $\pm U_C$. This voltage is applied to electrodes, which made it possible to change the phase delay between the arms, and, consequently, to control the splitting coefficient of the beam splitter. The accuracy of the splitting control is not worse as 0.1% in power.

Measurements of the noise signal at the output show an excess of the spectral power density of the detected quantum noise by an amount of more than 12 dB above the level of technical noise of the measuring system with a preamp in the band of more than 4 GHz [Fig. 3(a)]. The level of classical noise caused by random intensity noise (RIN) of the laser has a value much smaller than the quantum ones, which is confirmed by the proximity to the linear dependence characteristic of quantum shot noise [Fig. 3(b)]. The power level of the recorded quantum noise is in good agreement with the theoretical estimation, which predicts a linear growth of the output electrical power P as a function of the optical power P_{opt} of local oscillator:

$$N(f) = 2qP_{\text{opt}}AR_0|H_{\text{pd}}^2(f)|, \quad (21)$$

where $N(f)$ is the spectral power density, q is the electron charge, P_{opt} is the power on the input of the photodiodes, A is the direct current sensitivity of the photodiodes, $H_{\text{pd}}(f)$ is the transfer function of the balanced photodetector, R_0 is the output loading resistor of the balanced detector. As can be seen from Fig. 3(b), the experimental dependence has a form close to linear.

In our opinion, it is interesting to compare the potential rate of generating a sequence of random numbers using various realizations of noise sources. There are many types of such sources known in the literature [1], so we consider only those that use the balanced detection and the use of quantum noise as a source of entropy. For such a comparison, one can use the methodology [8], according to which the upper limit of the rate of random-number generation C is determined from the Nyquist theorem:

$$C = 2\Delta F \log_2 V, \quad (22)$$

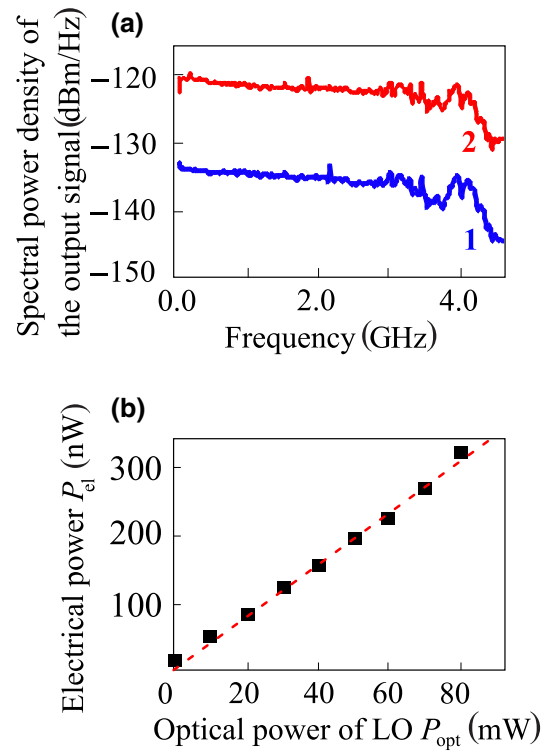


FIG. 3. Experimental results. (a) The spectral power density $N(f)$ at the output of balanced detector. 1: local oscillator “off”; 2: local oscillator “on”; (b) the electrical power P_{el} at the output of the balanced detector as a function of optical power P_{opt} of the local oscillator (LO). The red dotted line shows theoretical predictions of expression (21).

where ΔF is the bandwidth of the spectrum, and $V = 2^n$ is the quantization level for digitization resolution n . Then, for the case when a 16-bit analog-to-digital converter (ADC) is used, and the frequency band ΔF is from 2.5 to 3 GHz for the average of 10 dB of quantum to classical signal-to-noise ratio (QCNr) clearance, the estimation

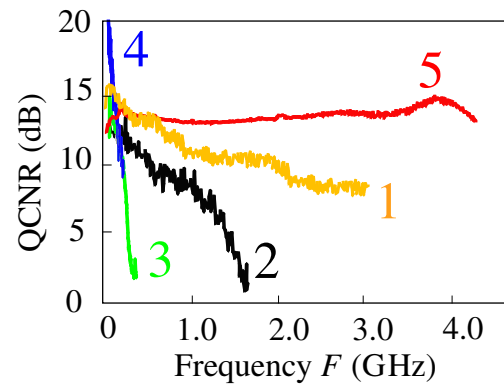


FIG. 4. Dependence of QCNr on frequency for different realizations of the quantum-noise generator. 1—[8], 2—[9], 3—[10], 4—[19], 5—our realization.

of the potential speed of extraction up to 70 Gbit/s random bits out of detector was obtained in Refs. [8,19].

From the experimental data presented in Fig. 3(a) it can be seen that the average of 12 dB of quantum to classical signal-to-noise ratio clearance has a frequency band of at least 4.0 GHz. Provided that a similar 16-bit ADC is used, it is possible to obtain, for our case, an upper estimation of the potential extract speed of at least 110 Gbit/s.

Obviously, the bandwidth has the greatest influence on the generation speed, and not the bit depth of the ADC. Therefore, we demonstrate, Fig. 4, that shows the dependences of QCNR for different realizations of quantum-noise sources on frequency for various implementations of quantum-noise sources [8–10,16]. These data are obtained by us through the appropriate processing of experimental data published in the listed works.

In the early 2010s, the generation rate achieved in Ref. [4] was 6.5 Mbits/s, and the potential was estimated as 200 Mbits/s, further in Ref. [8,19] the potential was estimated as 70 Gbits/s. In Ref. [9], for different types of ADC transformation, the generation rate achieved was 6 Gbits/s and 12 Gbits/s with the used spectral band 1.4 GHz. In Ref. [10] with the spectral range 120–140 MHz, the estimated speed of generation was reported as 1 Gbit/s. In Ref. [20] the reported speed of generation was 43 Mbit/s. It should be noted that the estimates given depend significantly on the number of ADC sampling levels and postprocessing algorithms. Nevertheless, the general trend of the connection of the increase in the generation rate with the bandwidth is obvious.

IV. CONCLUSION

We design and experimentally implement a quantum-noise source with remarkable characteristics. Three factors mainly determine the broadband source with a spectral bandwidth of more than 3 GHz.

First of all, such a broad generation band turns out to be possible due to the integrated-optical chip-based implementation of homodyne detection with the field mixer in the form of Y branch. It should be noted that, in contrast to traditional volumetric beam splitters or waveguide X couplers, the reflection and transmission coefficients of which depend quite critically on the the light wavelength [21], integrated optical Y branches are much more broadband elements. Thus, the spectral width of our generator is determined by the spectral characteristics of the detectors, not the beam splitters. This factor allows us to build a theory without considering the spectral dependence of the beam-splitter coefficients.

The second factor that makes it possible to achieve record results is developing a feedback loop that allows us to quickly and accurately control the delay in the arm of the Mach-Zehnder interferometer. As shown in the theoretical part of the paper, fine tuning of the balance allows getting

rid of the influence of classical noises in the system. The presence of asymmetric losses in the interferometer channels leads to degeneration of interference and the uncompensated currents proportional to the homodyne intensity mixing into the signal. Even a weak asymmetry can significantly impair the signal visibility due to large values of the homodyne amplitude. Controlling the interference phase using a feedback loop enables the achievement of the visibility of the quantum-noise signal above the classical noise by more than 12 dB.

It should be noted that if we imagine an ideal situation in which there are no classical noises in the system, then the asymmetry of the beam splitter does not worsen the observation parameters of quantum noise but rotates only the observation basis, which is not significant for symmetric noise distribution. Correctness of the quantum-mechanical description of the measurement in the presence of a feedback loop should also be discussed here. It is a well-known situation when feedback stabilizes the photoelectron flux but degrades the noise characteristics of light that produce this flux [22–24]. In the mentioned case, the direct connection between the operators of the light's quadratures and the photocurrent's operator is lost. There is no such problem in our case since the feedback controls not the quantum system but the classical one.

Finally, the third factor is the experimental selection of detectors with the closest possible characteristics. The selection of suitable photodiodes is an essential factor in improving the performance of the circuit, and we suggest that it is this block of the circuit that define cut-of frequency of the spectral characteristics of the device as a whole.

ACKNOWLEDGMENTS

The development of the technique for photonic shot-noise measurements is funded by the Ministry of Science and Higher Education of the Russian Federation, State Assignment No. 2019-0923.

-
- [1] M. Herrero-Collantes and J. C. Garcia-Escartin, Quantum random number generators, *Rev. Mod. Phys.* **89**, 015004 (2017).
 - [2] A. V. Gleim, V. V. Chistyakov, and O. I. Bannik, Sideband quantum communication at 1 Mbit/s on a metropolitan area network, *J. Opt. Tech.* **84**, 362 (2017).
 - [3] Y. Liu, Q. Zhao, M.-H. Li, J.-Y. Guan, Y. Zhang, B. Bai, W. Zhang, W.-Z. Liu, C. Wu, and X. Yuan, *et al.*, Device-independent quantum random-number generation, *Nature* **562**, 548 (2018).
 - [4] C. Gabriel, C. Wittmann, D. Sych, R. Dong, W. Mauerer, U. L. Andersen, C. Marquardt, and G. Leuchs, A generator for unique quantum random numbers based on vacuum states, *Nat. Photonics* **4**, 711 (2010).

- [5] T. Symul, S. M. Assad, and P. K. Lam, Real time demonstration of high bitrate quantum random number generation with coherent laser light, *Appl. Phys. Lett.* **98**, 231103 (2011).
- [6] T. Gehring, C. Lupo, A. Kordts, D. S. Nikolic, N. Jain, T. Rydberg, T. B. Pedersen, S. Pirandola, and U. L. Andersen, Homodyne-based quantum random number generator at 2.9 Gbps secure against quantum side-information, *Nat. Commun.* **12**, 605 (2021).
- [7] H. Zhou, P. Zeng, M. Razavi, and X. Ma, Randomness quantification of coherent detection, *Phys. Rev. A* **98**, 042321 (2018).
- [8] J. Y. Haw, S. M. Assad, A. M. Lance, N. H. Y. Ng, V. Sharma, P. K. Lam, and T. Symul, Maximization of Extractable Randomness in a Quantum Random-Number Generator, *Phys. Rev. Appl.* **3**, 054004 (2015).
- [9] B. Xu, Z. Chen, Z. Li, J. Yang, Q. Su, W. Huang, Y. Zhang, and H. Guo, High speed continuous variable source-independent quantum random number generation, *Quantum Sci. Technol.* **4**, 025013 (2019).
- [10] L. Huang and H. Zhou, Integrated Gbps quantum random number generator with real-time extraction based on homodyne detection, *JOSA B* **36**, B130 (2019).
- [11] Q. Zhou, R. Valivarthi, C. John, and W. Tittel, Practical quantum random-number generation based on sampling vacuum fluctuations, *Quantum Eng.* **1**, e8 (2019).
- [12] F. Raffaelli, G. Ferranti, D. H. Mahler, P. Sibson, J. E. Kennard, A. Santamato, G. Sinclair, D. Bonneau, M. G. Thompson, and J. C. F. Matthews, High speed continuous variable source-independent quantum random number generation, *Quantum Sci. Technol.* **3**, 025003 (2018).
- [13] Y. Shi, B. Chng, and C. Kurtsiefer, Random numbers from vacuum fluctuations, *Appl. Phys. Lett.* **109**, 041101 (2016).
- [14] Y. Shen, L. Tian, and H. Zou, Practical quantum random number generator based on measuring the shot noise of vacuum states, *Phys. Rev. A* **81**, 063814 (2010).
- [15] V. J. Urick, J. D. McKinney, and K. J. Williams, *Fundamentals of Microwave Photonics* (John Wiley & Sons, Hoboken, NJ, 2015), 457.
- [16] M. Izutsu, Y. Nakai, and T. Sueta, Operation mechanism of the single-mode optical-waveguide Y junction, *Opt. Lett.* **7**, 136 (1982).
- [17] O. Alibart, V. D'Auria, M. De Micheli, F. Doutre, F. Kaiser, L. Labonte, T. Lunghi, E. Picholle, and S. Tanzilli, Quantum photonics at telecom wavelengths based on lithium niobate waveguides, *J. Opt.* **18**, 104001 (2016).
- [18] A. Petrov, A. Tronev, P. Agruzov, A. Shamrai, and V. Sorotsky, System for Stabilizing an Operating Point of a Remote Electro-Optical Modulator Powered by Optical Fiber, *Electronics* **9**, 1861 (2020).
- [19] Z. Zheng, Y. Zhang, W. Huang, S. Yu, and H. Guo, 6 Gbps real-time optical quantum random number generator based on vacuum fluctuation, *Rev. Sci. Instrum.* **90**, 043105 (2019).
- [20] Y.-Y. Hu, Y.-Y. Ding, S. Wang, Z.-Q. Yin, W. Cheng, D.-Y. He, W. Huang, B.-J. Xu, G.-C. Guo, and Z.-F. Han, Compact quantum random number generation using a linear optocoupler, *Opt. Lett.* **46**, 133175 (2021).
- [21] S. M. Barnett, J. Jeffers, A. Gatti, and R. Loudon, Quantum optics of lossy beam splitters, *Phys. Rev. A* **57**, 2134 (1998).
- [22] T. Golubeva, Yu. Golubev, and D. Ivanov, Induced photon statistics in three-level lasers, *Phys. Rev. A* **75**, 023815 (2007).
- [23] A. Masalov, A. Putilin, and M. Vasilyev, Sub-Poissonian light and photocurrent shot-noise suppression in closed optoelectronic loop, *J. Mod. Opt.* **41**, 1941 (1994).
- [24] H. Wiseman and G. Milburn, Squeezing via feedback, *Phys. Rev. A* **49**, 1350 (1994).